

Ultrafast and slow luminescence decays at energy transfer from impurity-bound excitons

M.I. Danilkin^{a,b,*}, N. Yu. Vereschagina^c, Yu. G. Vainer^{b,c}, M.V. Kochiev^a, S.A. Ambrozevich^a, I. Romet^d, H. Mändar^d, A.N. Morozov^e, Yu. A. Repeev^c, D.A. Spassky^{d,f}, A.V. Shutov^a, L.V. Seleznev^a, D.V. Mokrousova^a, A.S. Selyukov^{a,g,h,i}

^a P.N. Lebedev Physical Institute of the Russian Academy of Sciences, 53 Leninsky Prospect, 119991 Moscow, Russia

^b Moscow Institute of Physics and Technology (State University), 9 Institutskii Per., 141700 Dolgoprudny, Moscow Region, Russia

^c Institute of Spectroscopy of the Russian Academy of Sciences, 5 Fizicheskaya Str., 108840 Troitsk, Moscow, Russia

^d Physics Institute of the University of Tartu, W. Ostwaldi tn. 1, 50411 Tartu, Estonia

^e Mendeleev University of Chemical Technology, 9 Miusskaya Sq., 125047 Moscow, Russia

^f Skobeltsyn Institute of Nuclear Physics (SINP MSU), M.V. Lomonosov Moscow State University, 1-2 Leninskiye Gory, 119991 Moscow, Russia

^g Bauman Moscow State Technical University, 5/1 2-ya Baumanskaya Str., 105005 Moscow, Russia

^h All-Russian Institute for Scientific and Technical Information (VINITI) of the Russian Academy of Sciences, 20 Usievicha Str., 125190 Moscow, Russia

ⁱ Moscow Polytechnic University, 38 Bolshaya Semyonovskaya Str., 107023 Moscow, Russia

ARTICLE INFO

Keywords:

Impurity-bound exciton

Ultrafast luminescence

Li₂B₄O₇: Sn/Mn

Li₂B₄O₇: Cu/Mn

Li₂B₄O₇: Mn

ABSTRACT

Different types of ultrafast radiative transitions are considered. The most interesting among them is the case when the radiative transition is accelerated by the configurational transformation of a structural unit where it occurs. Impurity-induced VUV excitation bands of doped Li₂B₄O₇ are attributed to the creation of impurity-bound excitons. When Mn²⁺ is involved into exciton recombination, the radiative transition in the Mn²⁺ 3d⁵ configuration is accelerated and occurs on a sub-nanosecond time scale. Excitation within the UV bands is connected with energy transfer from the structural units formed by the sensitizers (Cu, Sn) and oxygen to Mn²⁺. In this case, Mn²⁺ transitions are not accelerated since its excited state appears after complete relaxation of excitation in the corresponding sensitizer's unit. Pulsed cathodoluminescence decays are rather slow due to very slow transport of electron-hole pairs and excitons in Li₂B₄O₇.

1. Introduction

Fast scintillators are in demand for registration of events in nuclear physics as well as for medical imaging (positron-emission tomography, PET) [1–3]. The spatial resolution of time-of-flight measurements depends on the temporal resolution of the entire system. A scintillator which encounters radiation is the first element of such system. The faster is the response of the scintillator, the better is the resulting spatial resolution.

The present study discusses the possible approaches to obtaining fast scintillators, while an ultimate recipe is yet to be developed.

Sub-nanosecond radiative transitions are beyond the Born-Oppenheimer approximation unless the motion of nuclei is taken into account. In the frame of the “pure adiabatic” approximation, the fastest allowed radiative transitions should occur in several nanoseconds. Yet, examples of faster luminescence are well-known, and we shall mention them here.

The fastest one, intra-band luminescence, is connected with the radiative transitions of hot electrons or hot holes between the levels of the conduction or valence band of a crystal, respectively [4,5]. This process is limited in time by thermalization of carriers (which usually occurs on a picosecond time scale). Intra-band luminescence has a relatively low yield (10⁻⁴–10⁻³ photons per an electron-hole pair) [4]. The photon yield in the near-infrared region can be somewhat higher, especially for materials with low energy of optical phonons [5].

Another kind of fast luminescence is called cross-luminescence. It is similar to the hole intra-band luminescence, but concerns radiative transitions from the valence band to the upper core electronic levels in the deeper part of the valence band [6]. Such transitions occur when a hole appears at the core level, with an electron being extracted to conduction band by interaction with the incident radiation. Transitions produce photons effectively when there is a secondary band-gap between the valence band and the upper core levels, and this band is narrower than the main band-gap. The latter is necessary for the

* Corresponding author.

E-mail address: mihhail.danilkin@yandex.ru (M.I. Danilkin).

radiated photons to escape the material without reabsorption. This restriction should exclude also strong absorption of photons due to creation of impurity-bound excitons when the energy of photons is slightly smaller than the energy of the main band-gap. Discovered and studied first in BaF₂, this kind of luminescence shows fast decay (about 0.8 ns in BaF₂) and sufficiently high yield, so BaF₂ was even used in early PET machines [7]. Further studies revealed the cross-luminescence in different A^{II}B^{VII}, A^IB^{VII} and mixed (A^I-A^{II})B^{VII} compounds [8]. Cross-luminescence is intensively studied nowadays and has been reported recently in LaF₃ [9] and K₂SiF₆ [10], with the decay being extremely fast in the latter case (two exponentials with decay times of 0.08 ns and 0.23 ns).

Another example of fast luminescence is the luminescence involving impurity-bound and self-trapped excitons (IBE and STE). We need to mention here also the concept of giant oscillator strength initially suggested to explain near-edge absorption [11] and then extended to the IBE-related luminescence [12]. The idea of the oscillator strength came from the single-electron approximation. The unusually intense absorption of incident light with the energy slightly below energy gap E_g ("pre-spectral" bands) was described in terms of the giant oscillator strength (GOS) [11]. This idea is based on the fact that the wavefunction of IBE spreads over many atomic units, so it involves these units into the transition, forcing their action as a coherent dipole array and "stealing" the oscillator strength from this array. The oscillator strength of the IBE increases by a factor of 10^3 to 10^4 compared with the free exciton oscillator strength. Later, the idea of GOS was revisited in connection with the IBE luminescence in CdS and ZnO [12,13], and a clear formulation was given: the IBE oscillator strength is N times higher than that of the free exciton, where N is the number of coherently acting units covered by the IBE wavefunction. The coherence volume is found to be affected by temperature since phonon scattering destroys the coherence and limits the coherence volume [13]. Later, a very short decay time (15 ps at room temperature) was obtained in ZnO single crystals heavily doped with In (1.6×10^{18} atoms/cm³) [14]. In the latter case, the GOS concept seems to be irrelevant, as the decay time is very short even at room temperature. Moreover, the coherence volume is also limited by the impurity distribution in the heavily doped material. Hence, some other reason should be found to explain the short decay time here.

Consider some other interesting cases of very short decay times which can help in understanding the origin of ultrafast radiative transitions. Thus, a very short decay time (1 ps) was observed for singlet STEs in lithium niobate [15]. Locally decaying singlet STEs cannot hop through the crystal lattice due to a very short intrinsic decay time, and their decay time does not depend on temperature [15]. The STEs are located at niobium-oxygen octahedra, and obviously should produce changes in the geometry of these structural units. As a rule, the charge-transfer transitions should be accompanied by transformations in the geometry of the unit where they appear. This is caused by electrostatic interactions, and occurs on the femtosecond time-scale. Thus, the formation time of STEs in LiNbO₃ is ≤ 200 fs [15]. The involved chemical bonds and positions of nuclei undergo transformation during such a short time. When the excited configuration returns to the ground state, the excitation energy is released in different forms, including photon emission in extremely short time interval which is limited actually only by the uncertainty principle: $\Delta E \Delta t \geq \hbar/2 \approx 0.329$ eV · fs. The uncertainty in the energy is connected with the fact that the phase trajectory of the entire system before the photon is born cannot be defined and is of no matter for the photon creation, except for the geometry of the configuration. Generally, the Stokes shift could be a very rough measure of ΔE , so the photon can be born generally on the femtosecond time scale. What concerns the observed lifetime of the excited state, it refers to the prologue of the radiative transition when the system tries to find the configuration suitable to create the photon with the maximum probability. This concept can be related to the complex systems where the radiative transition is only a part of the

more general transition between the configurations which differ in the geometry of chemical bonds.

Localization of excitons is essential for short decay times. There are different means of such localization, from quantum confinement in quantum dots to specially designed layered materials. The latter case is illustrated in [16] where layered mixed-anion compounds Sr₂ScCuSeO₃ and Sr₃Sc₂Cu₂Se₂O₅ were studied. The excitonic luminescence decays bi-exponentially in these materials, with the typical decay times of 25–30 ps and 100 ps. The observed luminescence suffers, however, from thermal quenching [16]. The next and the most interesting example of ultrafast luminescence is that of Mn²⁺ in perovskite-like CsMnBr₃ nanocrystals [17]. Usually Mn²⁺ luminescence decays very slowly due to forbidden radiative transitions in the $3d^5$ configuration. However, this is not true in CsMnBr₃ where the Mn²⁺ luminescence decay time is 605 ps in nanocrystals and 550 ps in the bulk material [17]. At the same time, a high quantum yield (54% for nanocrystals and 6.7% for bulk) at room temperature excludes quenching as the nature of the observed ultrafast decay. The authors suggest that small Mn-Mn distances play essential role in the decay accelerating [17], however, the release of selection rules due to spin interactions usually can decrease the decay time to several nanoseconds, and not faster [18]. So, the reason for ultrafast Mn²⁺ luminescence decay in CsMnBr₃ could be the transformation of the cluster geometry at excitation, with the system returning to the ground state both radiatively and non-radiatively, and this process involving changes in the system geometry. Very fast transitions between the upper levels in the Mn²⁺ $3d^5$ configuration [17] favour this idea in principle.

The idea of the present study is to check whether the radiative transitions of Mn²⁺ can be forced due to energy transfer from the impurity-bound exciton created nearby. Lithium tetraborate (LTB) doped with Mn and co-doped with Sn or Cu was selected for this purpose. LTB has rather strong directed chemical bonds in the B–O framework and rather ionic Li–O bonds [19]. So, the exciton created in the B–O framework should produce essential deformation of chemical bonds, and this is a key factor for accelerating the radiative transitions. The samples under investigation were thoroughly characterized previously [19,20], which largely assists the present study.

2. Experimental

The samples are prepared in the form of ceramics using the technology described elsewhere [19]. Lithium tetraborate is produced by the reaction of a saturated solution of hot boric acid (reagent grade, purchased from ETIMADEN-EtiProducts Ltd.) with lithium carbonate (crystal grade, purchased from Chimmed Group). A small amount (1–2 wt.% relative to the Li₂B₄O₇ product) of SiO₂ is added to the boric acid solution. This component acts as a binder, flux, and also as a water-repelling agent [21]. Functional impurities are added either in a single stage or in two stages. The first impurity (in the form of aqueous solutions of Cu, Sn, or Mn sulphates) is added dropwise during the synthesis of the lithium tetraborate. A uniform distribution of the impurity is achieved by constant intense stirring not only during the reaction but also until the product is aged and water is mostly evaporated. The paste-like product is further dried for 15–18 h at 105 °C in air using a drying chamber. Then, the residual H₂O and CO₂ are removed by annealing at 580–500 °C under an argon flow. The obtained material is grinded. In the case of the two-stage doping, the second impurity (Mn) is added in the form of a MnSO₄ aqueous solution; then, after mixing and additional grinding, the material is dried and annealed once again. The tablets are produced from the obtained composition under a pressure of $1.5–2 \times 10^3$ kg/cm² at room temperature. Then, the tablets go through the final sintering at 880–890 °C in an argon atmosphere.

In this study, we explore three materials, LTB:Sn_{0.30} + Mn_{0.20}, LTB:Cu_{0.30} + Mn_{0.15}, and LTB:Mn_{0.14}. The added amounts of impurities specified in the subscripts are given in mol.%. The real impurity

concentration is smaller, since it is distributed between $\text{Li}_2\text{B}_4\text{O}_7$ microcrystals and the glass-like binder. The obtained ceramics consists of small single crystals of $\text{Li}_2\text{B}_4\text{O}_7$ (0.010–0.100 mm in size) obduced and glued together with a glassy binder. The thorough characterization of the obtained samples has been provided elsewhere [19]. The phase analysis detected tetragonal $\text{Li}_2\text{B}_4\text{O}_7$ to be the dominating phase in the samples. Besides that, a small amount of α -quartz is observed, which obviously results from partial crystallization of the added SiO_2 [19].

The uniformity of the impurity distribution in the samples has been explored using the energy-dispersive X-ray (EDX) analysis. The EDX mapping demonstrates that all impurities are distributed uniformly, except for Sn, which is partially concentrated in the glassy binder due to good compatibility with SiO_2 [19].

The photoluminescence (PL) and PL excitation spectra are studied using different setups equipped with either xenon or deuterium arc lamp, two monochromators (one used in the excitation channel, and the other in the emission registration channel), and photomultiplier tube detectors. The excitation spectra measured with different setups are joined together by matching their overlapping parts. The instrumentation for optical experiments is described in detail elsewhere [19]. Spectrally-resolved luminescence decays and time-resolved spectra are measured using Coherent Mira 900 Ti:Sa lasers equipped with external non-linear crystals for frequency doubling. The frequency of the incident frequency-doubled light is doubled once more at the edges of the microcrystals at the boundaries between $\text{Li}_2\text{B}_4\text{O}_7$ and the glass-like binder [19]. This makes the excitation bands below 200 nm accessible by the laser light source with a picosecond pulse duration. The excitation laser pulse energy is 0.01 nJ (after frequency-doubling by the external crystal). In order to select and excite a suitable microcrystal in the ceramic sample, micro-objectives and cameras are used to observe the luminescence visually during the excitation adjustment. To measure spectrally resolved luminescence decays, the emission of the sample is focused onto the entrance slit of a monochromator combined with a Hamamatsu C10600-10B streak camera. Time-resolved luminescence spectra are measured at the excitation pulse energy of 0.03 nJ using an iHR550 monochromator and a SPCM-AQR single-photon avalanche diode (Perkin-Elmer) coupled to a custom-made time-gated photon counter with a time window of 2.6 ns. The time window is moved by cable delays to either the start (“fast window”) or the middle (“slow window”) of the decay process.

Pulsed cathodoluminescence (PCL) is excited by a Radan-expert portable pulsed electron accelerator (2 ns pulse duration, 60 A amplitude, 260 keV maximum electron energy, energy distribution is peaked at 110–120 keV) and measured with an Ocean Optics Maya 2000 Pro spectrometer (integration time is 50 ms). The PCL decays are measured at 600 nm, with the luminescence of the sample being transmitted to the entrance slit of an MDR-3 monochromator by a quartz waveguide with a length of 4 m, which provides a delay of 20 ns. This delay is required to skip the electromagnetic interference produced by the excitation pulse. A FEU-100 photomultiplier connected with transimpedance amplifier based on an ADA4817 circuit, and a Tektronix TDS3054C digital oscilloscope provide the instrumental response time of 5.7–5.8 ns. The instrument response function (IRF) was obtained using a PicoQuant PDL800-B pulsed laser (405 nm, 75 ps, 40 MHz). To measure the IRF in the same geometry, the laser emission was directed to the LTB tablet which was placed in the Radan-expert camera as in the PCL measurements.

3. Results and discussion

3.1. Photoluminescence and excitation

The PL of Mn^{2+} in LTB is well-known, it appears as a band peaked at 2 eV in Fig. 1. It is attributed to the spin- and parity-forbidden transitions within the $3d^5$ configuration of Mn^{2+} . The shape and position of this band, which originates from Mn^{2+} at Li^+ positions in

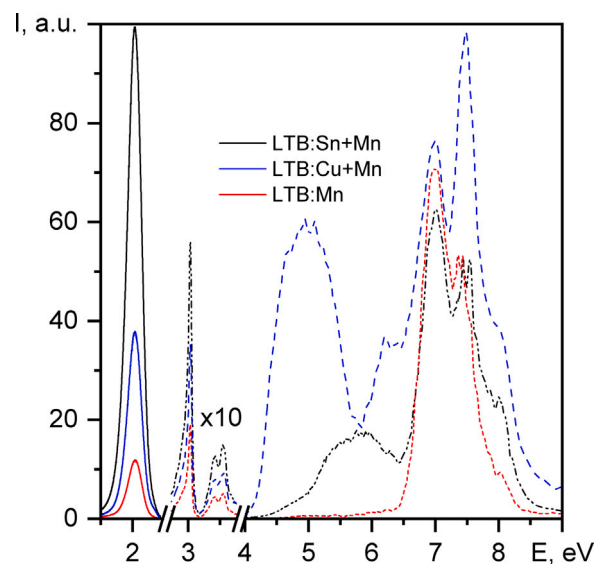


Fig. 1. Mn^{2+} emission (solid lines) and excitation spectra (dashed lines).

LTB, is independent of the excitation means and wavelength, as well as registration time-scales (see also Fig. 2). This is due to the relatively ionic character of chemical bonds at these positions, so the electrons from the $3d^5$ configuration are not involved in the strong interactions with the surrounding atoms.

The excitation spectra of Mn^{2+} (see Fig. 1) can be divided into three different ranges. The first one (2.5–4.0 eV) is connected with the direct excitation of Mn^{2+} through forbidden transitions in the $3d^5$ configuration, and therefore consists of weak and relatively narrow lines. The second range (4.0–6.0 eV, further referred to as the UV range, or UV excitation bands) is connected with the energy transfer from sensitizers (either Cu or Sn) [19] but there is no acceleration of Mn^{2+} radiative transitions at excitation within these bands [19]. The third range (6–8 eV, further referred to as the VUV range, or VUV excitation bands) is the most interesting for our discussion, it contains intense structured bands which are similar for the three studied objects but yet different in some structural details and peak positions. In our previous study [19], these bands were attributed to direct creation of IBE which transfer energy to Mn^{2+} . The energy transfer from IBE includes the mechanism of acceleration of radiative transitions [19] which we shall discuss below.

The impurity-bound excitons are localized at complex centres comprising two impurity atoms which are built in the LTB structure in a different manner. These atoms meet together in the LTB lattice due to chemical reasons [19]. Namely, one impurity atom (Me_i) can be incorporated into the boron-oxygen framework which is rather rigid and based on the directed chemical bonds. Another impurity atom (Me_s) substitutes for Li and has rather ionic bonds with the surrounding oxygen atoms. In both cases, the LTB crystal lattice suffers from some distortions and irregularities which can be minimized by joining the differently incorporated impurity atoms together into complex centres. At this, Me_i incorporated into the framework demonstrates acceptor features, while Me_s substituting for Li demonstrates donor features [19]. Me_i incorporated into framework should be able to make rather rigid directed bonds with the oxygen atoms around [19]. The structure unit formed by Me_i with oxygen atoms is adopted by and also transformed to match the LTB lattice, which means that coordination, bond character, and the size of this unit is tuned to fit the boron-oxygen framework though the latter also becomes somewhat distorted. In the samples described in the present paper, Me_i is either Sn, or Cu, or Mn, and Me_s is either Mn_{Li} or Cu_{Li} . The BO_3 triangles adjacent to these closely spaced Me_i and Me_s are affected by electronic density

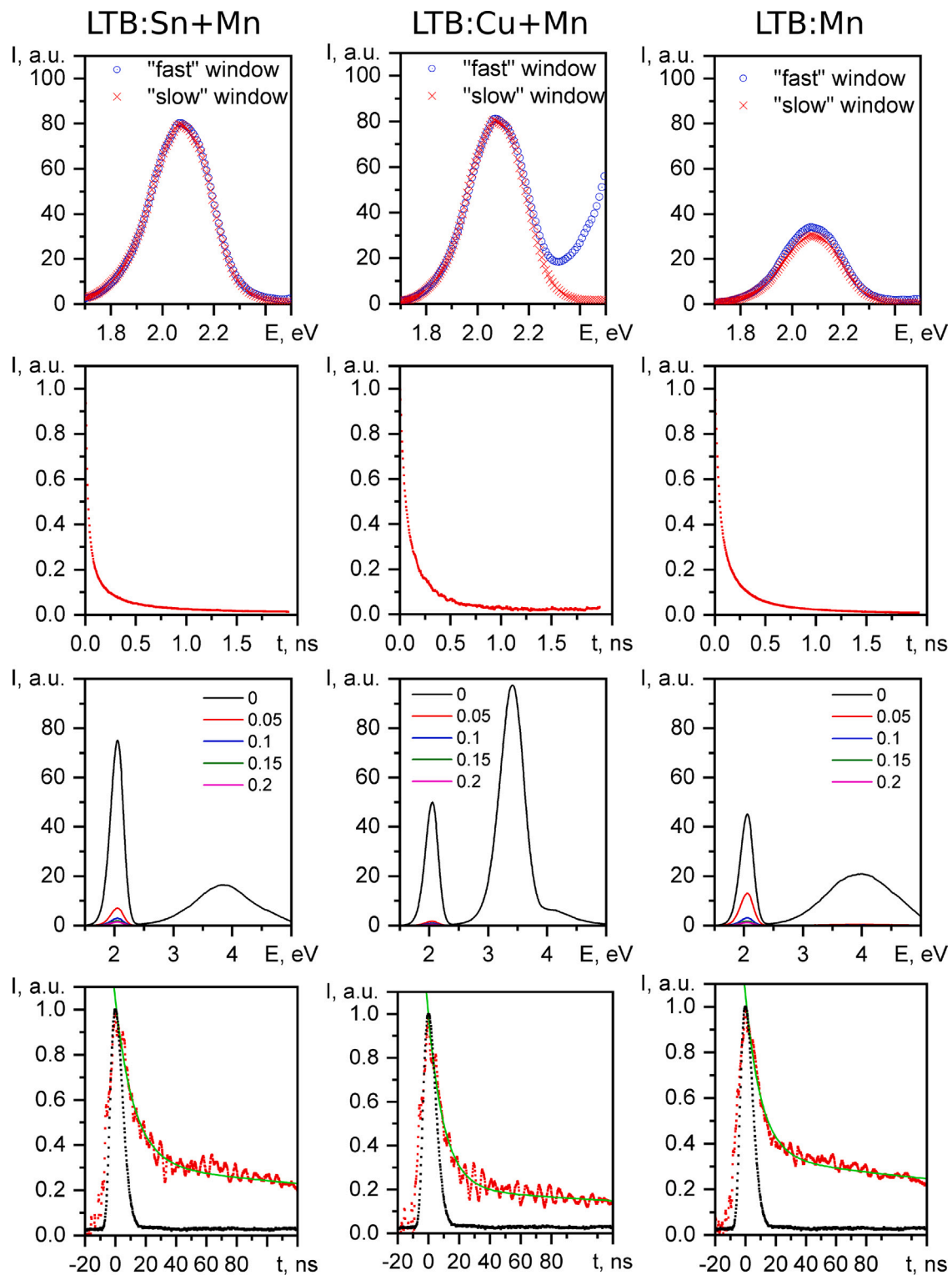


Fig. 2. First row: time-resolved spectra. Second row: photoluminescence decays at 600–620 nm obtained with laser excitation. Third row: PCL spectra with a step of 0.05 s. Fourth row: PCL decays (red), fitting (green), and IRF (black); for LTB:Sn + Mn $\tau_1 = 12.4$ ns and $\tau_2 = 372.8$ ns, for LTB:Cu + Mn $\tau_1 = 10.3$ ns and $\tau_2 = 365.7$ ns, for LTB:Mn $\tau_1 = 10.5$ ns and $\tau_2 = 361.7$ ns. (For interpretation of the references to colour in this figure legend, the reader is referred to the web version of this article.)

redistribution and are involved in complex centres participating in the excitation and energy transfer [19]. The regular exciton in LTB is known to be created at excitation near 8 eV [22], and the corresponding shoulder is observed in the excitation spectra of our samples (see Fig. 1). According to the DFT calculations [23], the lowest states of the LTB conduction band are composed of the excited electronic states of the BO_3 triangles (antibonding orbitals), while the upper valence band

states are mostly related to the BO_3 (and BO_4) ground states. Hence, the exciton in regular LTB lattice should be created mostly by the excitation of BO_3 triangles. When the electronic states of the BO_3 triangles are affected by the adjacent impurities, the excitation energy decreases, and, hence, the IBE is expected to be created just at excitation near 6–7.5 eV [19]. These VUV excitation bands are quite similar to the so called “pre-spectral” bands [11].

The amount of impurities in our samples is very low, one impurity atom per more than 60 crystal lattice units, with each unit containing 104 atoms. Therefore, casual grouping of impurities in the samples is practically impossible. Hence, the idea of natural forming complex luminescence centres $\text{Me}_i\text{-BO}_3\text{-Mn}_{iL}$ seems quite reasonable. These centres are responsible for the energy transfer to Mn^{2+} at excitation in the UV and VUV bands [19].

3.2. Time-resolved luminescence spectra and spectrally resolved decays

To study the luminescence spectra and spectrally resolved decay rates at VUV excitation, we used the frequency-doubled emission (350 nm) of the Mira 900 Ti:Sa pulsed laser obtained by virtue of an external non-linear crystal (BBO). This emission was focused on the sharp edge of the selected LTB microcrystal where it was frequency-doubled once again, thus producing light at 175 nm which was used immediately inside the microcrystal to excite the sample in the VUV spectral range. The details were published elsewhere [19], but we emphasize here one additional and very obvious proof of generation of the frequency-doubled light directly in the microcrystal. While Mn^{2+} luminescence can be excited by the incident light at 350 nm through forbidden transitions (producing such unpleasant side-effect as superluminescence of Mn^{2+} [19]), Cu^+ luminescence can be by no means excited by the incident light at 350 nm. On the contrary, the light (175 nm) that has been frequency-doubled at the edge of the microcrystal can excite Cu^+ luminescence (and also Mn^{2+} luminescence through similar energy transfer mechanisms). We obviously see a low-energy part of the Cu^+ luminescence band in the “fast window” (Fig. 2, first row, middle). Hence, the frequency-doubled light at 175 nm really appears in the microcrystal. What concerns the “slow window”, Cu^+ luminescence is absent here, and this indicates that Cu^+ luminescence excited in the VUV occurs mostly on the sub-nanosecond time scale. This, however, requires an additional study. It is interesting that Mn^{2+} spectrum is practically the same in the “fast” and in “slow” time windows. Only a very negligible shift towards higher energy can be observed in the “fast window” [19]. Probably, this is a result of inevitable Mn^{2+} superluminescence which contributes to the Mn^{2+} spectrum measured in the “slow window”, thus making the spectrum narrower. At the same time, the decays measured with a streak-camera demonstrate extremely short decay times for all three samples:

LTB:Sn + Mn: $\tau_1 = 0.027$ ns (72.1%), $\tau_2 = 0.171$ ns (23.0%), $\tau_3 = 1.391$ ns (4.9%);

LTB:Cu + Mn: $\tau_1 = 0.046$ ns (58.0%), $\tau_2 = 0.210$ ns (39.5%), $\tau_3 = 7.976$ ns (2.5%);

LTB:Mn: $\tau_1 = 0.044$ ns (67.0%), $\tau_2 = 0.211$ ns (28.5%), $\tau_3 = 1.170$ ns (4.5%).

The third exponential was added for the only purpose to compensate for the processes on the nanosecond time scale which are connected with the inevitable contribution of the Mn^{2+} superluminescence (by our observation, its characteristic decay times are from nanoseconds to tens of nanoseconds, depending on the excitation density).

Mn^{2+} in LTB:Sn + Mn has the fastest decay on the sub-nanosecond time scale. This sample is also the most efficient under excitation with a pulsed electron beam (see below). However, all three samples demonstrate unusually fast decays under VUV excitation, and this requires an explanation. We return to the explanation below, while here we should emphasize that we attribute the VUV excitation bands to the direct creation of IBEs which further transfer the excitation energy to Mn^{2+} . Hence, the energy transfer to Mn^{2+} from the primarily created IBE should include also some mechanism of acceleration of the Mn^{2+} radiative transitions.

What concerns the slow (5.6 ms) decay rates of Mn^{2+} luminescence, such decays are observed at the excitation either through forbidden transitions in the $\text{Mn}^{2+} 3d^5$ electronic configuration or by means of energy transfer from some entities excited in the UV spectral range. The details and the results of the corresponding experiments are reported in our previous study [19].

3.3. Cathodoluminescence and cathodoluminescence decays

The accelerated Mn^{2+} transitions observed at excitation within the VUV bands is a very interesting phenomenon, however, it would be also interesting how fast is the luminescence of Mn^{2+} at excitation with a pulsed electron beam. The most essential time-limiting factor is transport of electron-hole pairs and excitons to the luminescence centres [1]. Do complex luminescence centres play any role in accelerating other stages of energy transfer? To make things clear, a rather complex investigation of the excitation dynamics in the material under study is required. However, a very simple technique can give an indicative guess, whether there is an effect of such complex centres on the PCL decay stages in the nanosecond time-scale.

The PCL spectra measured with a 50 ms interval and decays obtained after a single shot are presented in Fig. 2, in the third and fourth row, respectively. The IRF measured with a pulsed laser is also added to the decay plots. The PCL decays were approximated by two exponentials. The first decay time is 10–12 ns, and the second one is 360–370 ns. Such decay times can be connected with rather slow migration of excitons and correlated electron-hole pairs in the LTB since their dependence on the introduced impurity is not very pronounced. The IRF characteristic time is 5.7–5.8 ns, and there are some deviations at the very start of the PCL decays which follow the shape of the IRF. Hence, there could be some faster components in the PCL decay and this point requires an additional study. What concerns the millisecond range, the PCL of Mn^{2+} and Cu^+ in LTB:Cu + Mn decays faster than the PCL of Mn^{2+} in the other samples. An obvious factor should be taken into account, namely, the presence of a concurrent Cu^+ luminescence (see the strong luminescence band near 3.35 eV in Fig. 2). Cu^+ luminescence is very fast (this fact was mentioned before by other researchers [24]). The faster Mn^{2+} PCL decay could be the result of exhaustion of excitation energy by the faster Cu^+ luminescence. However, the faster and more efficient luminescence of Cu^+ needs some explanation as well. Here we return to the question posed above: is there any influence of impurities on the migration rates of excitations in LTB? We see that some stages of energy transfer occur faster when LTB is doped with Cu. One of the possible reasons could be, for example, a smaller size of the microcrystals in the ceramics. However, our previous study rejects this idea [19]. On the contrary, the smallest size and less uniform distribution of impurities (Sn) is characteristic of LTB:Sn + Mn which demonstrates a slower PCL decay. Hence, there should be some other reason. We can assume that the local environment of the complex centres containing Cu does play some role in the excitation energy transfer; however, the matter requires further investigations.

4. The model of ultrafast and slow Mn^{2+} luminescence decays

BO_3 triangles near impurities are excited in the VUV bands and thus IBEs are formed. Excitation of a BO_3 triangle is accompanied with the transfer of the electron density from oxygens to the central boron atom, which, in turn, changes the BO_3 configuration to a pyramid-like structure due to electrostatic forces. At this, extra electron from boron is transferred to Mn (most likely, to the $4s$ level), and some kind of dynamically created bond between Mn and B appears. The BO_3 configuration is still distorted, while the oxygens take an electron from Mn back, but an electron first delivered to the upper Mn^{2+} level is now removed from the background level (lying near the upper states of the valence band). This sequential charge transfer creates an excited Mn^{2+*} , with the BO_3 unit configuration still being distorted, as the charge transfer processes usually occur on the femtosecond time scale. Radiative transition $\text{Mn}^{2+*} \rightarrow \text{Mn}^{2+} + h\nu$ occurs together and simultaneously with the return of the BO_3 unit configuration to the initial state, which provides the acceleration of the radiative transition [19].

Excitation within the UV bands (this is applicable to LTB:Cu + Mn and LTB:Sn + Mn) is also connected with the charge transfer, but here it

occurs in the Me_i-O structure unit incorporated in the framework [19]. In this case the electron density is transferred from Me_i to oxygens, and it is accompanied with the structure distortion as well. While an electron becomes immediately accessible to Mn, a hole stays at Me_i , which is isolated from Mn by oxygens. Mn^{2+} excitation in this case is accomplished when a hole is also transferred to Mn, but this occurs due to relaxation of the excited Me_i-O structure unit. At this, excited Mn^{2+} radiatively returns to the ground state without assistance of any accelerating mechanism, and the radiative transition $Mn^{2+*} \rightarrow Mn^{2+} + h\nu$ is slow [19].

5. Conclusion

There are several types of ultrafast radiative transitions. Present study is concentrated on the case when the radiative transition is a part of the transition between configurations of a complex system, with the geometry of the latter being transformed in the course of the transition. Such transitions are characteristic of impurity-bound excitons in the compounds with rather rigid directed chemical bonds. The structural unit where exciton is localized should be capable of changing the geometry due to charge transfer between the atoms of the unit. When an impurity ion is completely involved into the exciton recombination, the radiative transition in the entire system (exciton+impurity) can be very fast due to simultaneous relaxation of surrounding atoms. The transition in the system as a whole involves simultaneously a radiative transition and a transition between two different configurations, and is accompanied with the charge transfer. This warrants the acceleration mechanism for the radiative part of the transition. The slow luminescence decay occurs when the excitation energy transfer to a luminescence centre is accomplished yet after the system configuration returns to the initial state, since there is no more acceleration mechanism of the radiative transitions in this case. This principle is illustrated with the luminescence of Mn^{2+} in lithium tetraborate sensitized by co-activators. Unusually fast radiative transitions observed on the picosecond time scale are connected with a tight interaction of Mn^{2+} with the impurity-bound exciton created nearby. Nevertheless, there is another limiting factor to be regarded for the development of fast scintillators — this is the time necessary to transfer excitons and geminate electron-hole pairs to luminescence centres [1]. Our measurements of pulsed cathodoluminescence decays demonstrated that lithium tetraborate has rather slow transport of excitations to the luminescence centres. However, it was a good choice for developing the models of the observed phenomena.

Declaration of competing interest

The authors declare that they have no known competing financial interests or personal relationships that could have appeared to influence the work reported in this paper.

Acknowledgements

S.A. Ambrozevich and A.S. Selyukov acknowledge the support from the Russian Science Foundation (project no. 17-72-20088-p) for performing the slow decay measurements. D.A. Spassky and I. Romet gratefully acknowledge the financial support from the Estonian Research Council, project PUT PRG111. Hugo Mändar appreciates the support of the European Regional Development Fund project “Emerging orders in quantum and nanomaterials” (No. TK134). A.V. Shutov acknowledges the support from grant no. MK-418.2022.1.2.

Authors are grateful to Dr M.A. Kazaryan (P.N. Lebedev Physical Institute, RAS) for helpful discussions.

References

- [1] P. Lecoq, M. Korzhik, A. Vasiliev, Can transient phenomena help improving time resolution in scintillators? *IEEE Trans. Nucl. Sci.* 61 (1) (2014) 229–234.
- [2] P. Lecoq, Pushing the limits in time-of-flight PET imaging, *IEEE Trans. Radiat. Plasma Med. Sci.* 1 (6) (2017) 473–485.
- [3] C. Tsoumpas, Why ultrafast is ultra-good, *Phys. World* 33 (6) (2020) 41–44.
- [4] D.I. Vaisburd, S.V. Kharitonova, Two types of fundamental luminescence of ionization-passive electrons and holes in optical dielectrics—Intraband-electron and interband-hole luminescence (theoretical calculation and comparison with experiment), *Russian Phys. J.* 40 (11) (1997) 1037–1060.
- [5] S. Omelkov, V. Nagirnyi, A. Vasil'ev, M. Kirm, New features of hot intraband luminescence for fast timing, *J. Lumin.* 176 (2016) 309–317.
- [6] P. Rodnyi, Core-valence band transitions in wide-gap ionic crystals, *Sov. Phys. Solid State* 34 (7) (1992) 1053–1066.
- [7] K. Ishii, H. Orihara, T. Matsuzawa, D.M. Binkley, R. Nutt, High resolution time-of-flight positron emission tomograph, *Rev. Sci. Instrum.* 61 (12) (1990) 3755–3762.
- [8] V. Vaněček, J. Páterek, R. Král, R. Kučerková, V. Babin, J. Rohlíček, R. Cala, N. Kratochvíl, E. Auffray, M. Nikl, Ultraviolet cross-luminescence in ternary chlorides of alkali and alkaline-earth metals, *Opt. Mater.: X* 12 (2021) 100103.
- [9] M. Cadatal-Raduban, A. Yoshikawa, L.V. Mui, M.H. Pham, T. Shimizu, N. Sarukura, T. Togashi, K. Yamanoi, Investigation of cross luminescence in lanthanum fluoride as a potential fast-response scintillator, *Japan. J. Appl. Phys.* 59 (5) (2020) 052005.
- [10] J. Saaring, E. Feldbach, V. Nagirnyi, S. Omelkov, A. Vanetsev, M. Kirm, Ultrafast radiative relaxation processes in multication cross-luminescence materials, *IEEE Trans. Nucl. Sci.* 67 (6) (2020) 1009–1013.
- [11] E. Rashba, G. Gurgenshvilii, Edge absorption theory in semiconductors, *Sov. Phys. Solid State* 4 (4) (1962) 759–760.
- [12] C.H. Henry, K. Nassau, Lifetimes of bound excitons in CdS, *Phys. Rev. B* 1 (4) (1970) 1628–1634.
- [13] J. Wilkinson, K. Ucer, R. Williams, Picosecond excitonic luminescence in ZnO and other wide-gap semiconductors, *Radiat. Meas.* 38 (4–6) (2004) 501–505.
- [14] M. Kano, A. Wakamiya, K. Sakai, K. Yamanoi, M. Cadatal-Raduban, T. Nakazato, T. Shimizu, N. Sarukura, D. Ehrentraut, T. Fukuda, Response-time-improved ZnO scintillator by impurity doping, *J. Cryst. Growth* 318 (1) (2011) 788–790.
- [15] A. Krampf, S. Messerschmidt, M. Imlau, Superposed picosecond luminescence kinetics in lithium niobate revealed by means of broadband fs-fluorescence upconversion spectroscopy, *Sci. Rep.* 10 (1) (2020).
- [16] Y. Iwasa, H. Ogino, D. Song, K. Yamanoi, T. Shimizu, J. Ueda, S. Tanabe, N. Sarukura, Luminescence properties of layered mixed-anion compounds $Sr_2ScCuSeO_3$ and $Sr_3Sc_2Cu_2Se_2O_{15}$, *Opt. Mater.* 84 (2018) 205–208.
- [17] J. Almutaq, W.J. Mir, L. Gutiérrez-Arzaluz, J. Yin, S. Vasylevskiy, P. Maity, J. Liu, R. Naphade, O.F. Mohammed, O.M. Bakr, $CsMnBr_3$: Lead-free nanocrystals with high photoluminescence quantum yield and picosecond radiative lifetime, *ACS Mater. Lett.* 3 (3) (2021) 290–297.
- [18] K. Yan, C. Duan, Y. Ma, S. Xia, J.-C. Krupa, Photoluminescence lifetime of nanocrystalline $ZnS:Mn^{2+}$, *Phys. Rev. B* 58 (20) (1998) 13585–13589.
- [19] M. Danilkin, N. Vereschagina, Y. Vainer, M. Kochiev, S. Ambrozevich, I. Romet, H. Mändar, A. Morozov, Y. Repeev, D. Spassky, A. Shutov, L. Seleznev, D. Mokrousova, A. Selyukov, Ultrafast and slow Mn^{2+} luminescence in lithium tetraborate, *J. Alloys Compd.* 883 (2021) 160852.
- [20] M. Danilkin, Y. Koksharov, I. Romet, V. Seeman, N.Y. Vereschagina, A. Zubov, A. Selyukov, Manganese agglomeration and radiation damage in doped $Li_2B_4O_7$, *Radiat. Meas.* 126 (2019) 106134.
- [21] G. Kitis, C. Furetta, M. Prokic, V. Prokic, Kinetic parameters of some tissue equivalent thermoluminescence materials, *J. Phys. D: Appl. Phys.* 33 (11) (2000) 1252–1262.
- [22] I.N. Ogorodnikov, V.A. Pustovarov, A.V. Kruzhalov, L.I. Isaenko, M. Kirm, G. Zimmerer, Self-trapped excitons in LiB_3O_5 and $Li_2B_4O_7$ lithium borates: Time-resolved low-temperature luminescence VUV spectroscopy, *Phys. Solid State* 42 (3) (2000) 464–472.
- [23] C. Santos, A. Lima, M. Lalic, Electronic structure and optical properties of lithium tetraborate detector calculated using semi-local exchange correlation potential, *Comput. Mater. Sci.* 95 (2014) 271–275.
- [24] B. Huy, V. Quang, M. Ishii, Radioluminescent mechanism of $Li_2B_4O_7:Cu$ crystal, *J. Lumin.* 130 (11) (2010) 2142–2145.